Multifunctional graphene oxide/biopolymer composite aerogels for microcontaminants removal from drinking water

Multifunctional graphene oxide/biopolymer composite aerogels for microcontaminants removal from drinking water

Alessandro Kovtun,[a,‡] Elisabetta Campodoni,[b,‡] Laura Favaretto,[a] Massimo Zambianchi,[a] Anastasio Salatino,[c] Stefano Amalfitano,[c] Maria Luisa Navacchia,[a] Barbara Casentini,[c] Vincenzo Palermo,[a,d,*] Monica Sandri,[b] Manuela Melucci[a,*]

Consiglio Nazionale delle Ricerche (CNR, Italy), a) Institute of Organic Synthesis and Photoreactivity (CNR-ISOF) via Piero Gobetti 101, 40129 Bologna, Italy, b) Institute of Science and Technology for Ceramics (CNR-ISTEC) Via Granarolo, 64 - 48018 Faenza (RA), c) Water Research Institute (CNR-IRSA) Via Salaria Km 29,300 C.P. 10- 00015 Monterotondo Stazione (RM), d) Chalmers University of Technology, Industrial and Materials Science, Hörsalsvägen 7A, SE-412 96 Goteborg, Sweden.

Abstract

Due to water depletion and increasing level of pollution from standard and emerging contaminants, the development of more efficient purification materials and technology for drinking water treatment is a crucial challenge to be addressed in the near future. Graphene oxide (GO) has been pointed as one of the most promising materials to build structure and devices for new adsorbents and filtration systems. Here, we analyzed two types of GO doped 3D chitosan-gelatin aerogels with GO sheets embedded in the bulk or deposited on the surface. Through combined structural characterization and adsorption tests on selected proxies of drinking water micropollutants, we compared both GO-embedded and GO-coated materials and established the best architecture for achieving enhanced removal efficiency toward contaminants in water. To evaluate the best configuration, we studied the adsorption capacity of both systems on two organic molecules (i.e.,

fluoroquinolonic antibiotics ofloxacin and ciprofloxacin) and a heavy metal (lead Pb^{2+}) of great environmental relevance and with already proved high affinity for GO. The Pb monolayer maximum adsorption capacity q_{max} was 11.1 mg/g for embedded GO aerogels and 1.5 mg/g in coated GO-ones. Only minor differences were found for organic contaminants between coating and embedding approaches with an adsorption capacity of 5-8 mg/g and no adsorption was found for chitosan-gelatin control aerogels without GO. Finally, potential antimicrobial effects were found particularly for the GO-coated aerogels materials, thus corroborating the multifunctionality of the newly developed porous structures.

Keywords. Graphene oxide aerogels, chitosan, drinking water, lead, antibiotics, adsorption

1. Introduction

Drinking water contamination is a major concern to be rapidly faced with new materials and technologies. More than 30000 chemicals with a variety of chemical structures and unknown long-term toxicity and effect on the ecosystems are introduced every day into the market and directly or indirectly released into our water resources. Due to the lack of efficiency for a complete removal of emerging contaminants by wastewater treatment technologies, their occurrence in drinking water is not uncommon (Riva et al., 2018; Lapworth et al., 2012). This creates an urgent need to design versatile purification systems (i.e. adsorbent, membranes) with wider selectivity, enhanced efficiency, which can be regenerated to tackle the removal of a wide range of contaminants in a sustainable way (Joseph et al., 2017). The recently proposed recast of the European drinking water Directive 98/83/EC (Recast, (2017) 753, 2017), includes revision of the current limits for a wide list of contaminants including organic molecules, metal ions and cultivable index microbial pathogens (Annex, (2017), 753). The concentration limits for some toxic substances have been reduced (i.e., Pb and Cr), some pollutants of raising concern have been added (i.e., perfluorinated compounds,

chlorate and chlorite, endocrine disrupting compounds) and proposed microbiological assessment methods were updated.

Moreover, emerging chemical contaminants, hardly removed by conventional treatment, represent additional threats for direct human consumption of treated waters (Lapworth et al., 2012; Hartmann et al., 2018). In Europe, the Directive 2008/105/EC introduced Environmental Quality Standards for a number of emerging pollutants to protect human and environmental health. The updated Watch List includes organic contaminants, such as pesticides, pharmaceuticals, perfluorinated compounds, personal healthcare products, and heavy metals (cadmium, lead, mercury and nickel) (EU Watchlist). Along with chemicals, there are also major risks associated with the occurrence of microbial pathogens and antimicrobial resistant microorganisms even at very low concentrations, which are known to negatively influence the provision of water for drinking purposes (Nappier et al., 2018).

Water contaminants are currently removed by different technologies that often need to be combined to guarantee the required level of purity, thus urgently calling for the development of multifunctional materials possibly capable of simultaneous removal of different species of contaminants.

Due to their high specific surface area and surface reactivity as compared to conventional bulk materials, nanomaterials show high potential in controlling heavy metals, organic pollutants and microorganism removal in drinking water (Simeonidis et al., 2016; Xu et al., 2018).

In particular, graphene oxide (GO) holds great potential in this field (Ersan et al., 2017; Wang et al., 2015; Sweetman et al., 2017; Baig et al., 2019). Indeed, GO represents a scaffold with π-π-interactions, hydrophobic interactions as activated carbons, but it also has polar chemical oxygen based chemical groups promoting higher hydrophilicity, electrostatic interaction, higher processability in water (Backes et al., 2020). Moreover, graphene-based nanosheets are also potentially ideal materials to intercalate/capture metal ions (Ji et al., 2019; Xu et al., 2017), hence

77 opening promising perspectives in batteries and supercapacitors applications (Mukherjeel et al.,
78 2018).
79 Finally, graphene has been studied also for its antibacterial properties, based on the mechanical
80 disruption and penetration of graphene platelets in the bacterial membrane (Zou et al., 2016).
81 However, despite such outstanding properties, their effect in drinking water has still to be properly
82 evaluated (Westerhoff et al., 2018; Troester et al., 2016). Removal of GO nanosheets from treated
83 water would not be trivial, thus their inclusion in 3D structures is required to avoid side
84 contamination.
85 Different graphene oxide-based 3D structures have been proposed and some of them have already
86 proved superior adsorption capability compared with Granular Activated Carbon (GAC), the
87 industrial standard for some metal ions and organic compounds (Yousefi et al., 2019). Moreover,
88 covalent chemical modification of the oxygen-based functionalities offers a powerful tool to tune
89 the selectivity of GO based structures (Good et al., 2016). Defining the best approach for supporting
90 GO on 3D structures is important to maximize the removal efficacy of the final composite.
91 Indeed, the interaction between GO and the organic molecules strongly depend on the exposure of
92 GO sheets to the water solutions, thus the processing conditions to prepare GO composites is
93 expected to strongly impact on the removal efficiencies and mechanism. We recently proved that
94 PSU-GO composites adsorption of organic molecules is effective in both embedded (Zambianchi et
95 al., 2017) or coated (Kovtun et al., 2019a; Kovtun et al., 2020) configurations with higher
96 performance for GO coated structures in which the interlayer distance between GO sheets can play
97 a role.
98 Along this line, we consider here gelatin-chitosan (GC) based aerogels (Barrios et al., 2019)
99 specifically designed to host GO and compare two different fabrication approaches, based on the
100 embedding of GO into aerogel or coating of GC. We evaluated mechanical stability, GO release and
101 efficiency of adsorption of the targeted contaminants from water.

Gelatin is a hydrophilic and water-soluble protein polymer, deriving from collagen hydrolysis, then completely biocompatible. Chitosan is a natural cationic polysaccharide, deriving from the deacetilation of chitin, the main component of crustacean's exoskeletons. Both these biopolymers, selected primarily for their chemical properties and ability to form 3D structures, are waste materials of the food industry and due to their plentiful alimentary use, are highly available, low-cost and suitable to respond to the concept of circular economy. Moreover, chitosan has been widely used in water treatment by itself or as a support of more active compounds (Yang et al., 2016) and it is particularly interesting also for its natural antimicrobial activity (Hosseinnejad et al., 2016).

Chitosan-gelatin blends can be suitably combined and processed by freeze-drying, to achieve aerogels of customised properties in terms of porosity, density, surface area availability and structures. Cross-linking between them have been shown to create irreversible covalent bonds deriving from the reaction between pendant carboxylic and amino groups. Chitosan improves mechanical properties and prevents degradation in water observed for simple blends (Shankar et al., 2017; Campodoni et al., 2019; Krishnakumar et al., 2018). Furthermore, due to the exposed amino groups, CG aerogels can interact and react with carboxylic and epoxides groups of GO (Poletti et al., 2020) allowing to obtain stable composite devices that attract great attention in the field of biotechnology (Zhang et al., 2017).

To unravel the actual exposure and efficacy of GO in both composites, we perform adsorption test on two organic molecules, ofloxacin and ciprofloxacin, and Pb ions for whom GO has already proved good adsorption capacity (Peng et al., 2017; Wan et al., 2016; Zhoun et al., 2015; Wan et al., 2016; Madadrang et al., 2012). Indeed, we recently demonstrated the great affinity of GO for fluoroquinolonic antibiotics that resulted in maximum adsorption capacity (q_{max}) higher than 300 mg/g for ofloxacin molecule for GO nanosheets (Kovtun et al., 2019a) and of about 31 mg/g for polysulfone-GO (Kovtun et al., 2019a) composites. Moreover, the removal of Pb by GO aerogel was previously tested and q_{max} was calculated to be as high as 158 mg/g according to Langmuir

model (Tabrizi et al., 2016). For sake of comparison with previous published data, we used these molecules as references to check if GO was effective for adsorption in the targeted configurations more suitable for drinking water treatments.

It should be noted that the selected contaminants are of great environmental concern. Indeed, US-Environmental Protection Agency is keeping a watchful eye onto possible Pb contamination after water crises induced by Pb contamination into piped waters (Roy et al., 2019; Levallois et al., 2018) and in Europe 98/83/EU Directive for water intended for human consumption is currently under discussion and Pb concentration now regulated at 10 μg/L is suggested to be lowered at 5 μg/L. On the other hand, ofloxacin and ciprofloxacin are fluoroquinolonic antibiotics, with ciprofloxacin included in the EU Watch List (EU Watchlist).. Antibiotics represent one of the emerging contaminants in groundwater (Lapworth et al., 2012), since. they are frequently detected in different aquatic environments within urban water cycles (waste, surface and drinking water (Sanseverino et al., 2018; Pharmaceuticals, 2011) (Patrolecco et al., 2018).

2. Materials and methods

2.1 Synthesis

Type A pig skin gelatin (Gel, G) in powder form (mesh 4, bloom 280) was purchased from Italgelatine (Cuneo, Italy). Low molecular weight chitosan (Chit, C) was supplied by Sigma-Aldrich (MO, USA). GO was prepared by Hummer method according to previously described procedure (Melucci et al., 2012). High-purity chemical reagents were purchased from Sigma-Aldrich. Ultrapure water (Milli-Q) was used for all experiments.

Synthesis of Gelatin-Chitosan aerogels as control in the embedding technique (CG-E):

A 2% w/w Gel solution was prepared dissolving 8 g in 400 mL of Milli-Q at 45 °C and a 2% w/w Chit solution was prepared dissolving 3.43 g in 171.42 mL of 1% acetic solution till its complete dissolution. Gel and Chit solutions were blended at room temperature for 15 min in order to obtain a Gel:Chit ratio of 70:30 and a final blend concentration of 2% w/w.

Blend hydrogel were freeze-dried putting into a specific home-made mould with a copper bottom and plastic wall, to perform a perfect vertical growth of ice crystal and following a specific freeze-drying cycle with a controlled freezing ramp (50 °C/h) until -40 °C and with a controlled heating ramp of 5 °C/h from 40 °C to -10 °C and to + 15 °C at 3°C/h. Dehydrothermal treatment (DHT) was carried out after freeze-drying to cross-link GC aerogels and improve their stability. Aerogels were introduced into an oven at 100 °C for 48h under vacuum (0.01 mbar).

Synthesis of CGGO-E. A 4% w/w Gel solution was prepared dissolving 8 g in 200 mL of Milli-Q at 45 °C and a 2% w/w Chit solution was prepared dissolving 3.43 g in 171.42 mL of 1% acetic solution till its complete dissolution. Gel and Chit solutions were blended at room temperature for 15 min in order to obtain a Gel:Chit weight ratio of 70:30. GO suspension was prepared dispersing 0.572 g in 228.5 mL of Milli-Q using a tip sonicator (Sonics, Vibra cell, VCX500, max power 500W, ampl. 40 % for 10 min). GO suspension was added in GC blend for 15 min in order to obtain a final blend concentration of 2% w/w and a GO:blend weight ratio of 5:95. The composite hydrogel GCGO-E was introduced into a specific home-made mould with a copper bottom and plastic wall and, after gelation, was freeze-dried by setting a specific freeze-drying cycle: a freezing ramp of 50 °C/h, until -40 °C and a controlled heating ramp of 5 °C/h from -40 °C to -10 °C and to 15°C at 3°C/h. The customised mould and process were essential to obtain a perfect vertical growth of ice crystals and thus an aligned structure in the dried composite aerogel. DHT treatment was carried out after freeze-drying to cross-link GCGO aerogels and improve their stability: the samples were introduced into an oven at 100 °C for 48h under vacuum (0.01 mbar).

Synthesis of Gelatin-Chitosan aerogels as control for the coating approach (CG-C). A 2% w/w Gel solution was prepared dissolving 8 g in 400 mL of Milli-Q at 45 °C and a 2% w/w Chit solution was prepared dissolving 3.43 g in 171.42 mL of 1% acetic solution till its complete dissolution. Gel and Chit solution were blended at room temperature for 15 min in order to obtain a Gel:Chit ratio of 70:30 and a final blend concentration of 2% w/w.

179 The GC hydrogel was introduced into a specific home-made mould with a copper bottom and
180 plastic wall and, after gelation, was freeze-dried by setting a specific freeze-drying cycle: a freezing
181 ramp of 50 °C/h, until -40 °C and a controlled heating ramp of 5 °C/h from -40 °C to -10 °C and to
182 15°C at 3°C/h. The customised mould and process were essential to obtain a perfect vertical growth
183 of ice crystals and thus an aligned structure in the dried aerogel. DHT treatment was carried out
184 after freeze-drying to cross-link GC aerogels and improve their stability. Samples were introduced
185 into an oven at 160 °C for 48h under vacuum (0.01 mbar).
186 **Synthesis of CGGO-C.** A 2% w/w Gel solution was prepared dissolving 8 g in 400 mL of Milli-Q
187 at 45 °C and a 2% w/w Chit solution was prepared dissolving 3.43 g in 171.42 mL of 1% acetic
188 solution till its complete dissolution. Gel and Chit solution were blended at room temperature for 15
189 min in order to obtain a Chit:Gel ratio of 30:70 and a final blend concentration of 2% w/w.
190 The CG hydrogel was freeze-dried was introduced into a specific home-made mould with a copper
191 bottom and plastic wall and, after gelation, was freeze-dried by setting a specific freeze-drying
192 cycle: a freezing ramp of 50 °C/h, until -40 °C and a controlled heating ramp of 5 °C/h from -40 °C
193 to -10 °C and to 15°C at 3°C/h. The customised mould and process were essential to obtain a
194 perfect vertical growth of ice crystals and thus an aligned structure in the dried aerogel. DHT
195 treatment was carried out after freeze-drying to cross-link CG aerogels and improve their stability.
196 Aerogels were introduced into an oven at 160 °C for 48h under vacuum (0.01 mbar).
197 GO suspension was prepared dispersing 0.572 g in 228.5 mL of Milli-Q using a tip sonicator
198 (Sonics, Vibra cell, VCX500, max power 500W, ampl. 40 % for 10 min). The GO suspension was
199 dropped into GC aerogels in order to obtain a final GO:blend weight ratio of 5:95 and maintained at
200 room temperature for 15 min. Dried aerogels was obtained through another freeze-drying with the
201 same cycle performed before (freezing ramp of 50 °C/h until -40 °C and with a controlled heating
202 ramp of 5 °C/h from -40 °C to -10 °C and to 15°C at 3°C/h).
203 **2.2 SEM and porosity**

The scaffold morphology and the pore size were observed by environmental scanning electron microscopy (ESEM) (Quanta 600 FEG, FEI Company, Hillsbrono, OR). The specimens were mounted on aluminium stubs using carbon tape, and they were covered with a coating of Au using coating units Polaron Sputter Coater E5100 (Polaron Equipment, Watford, Hertfordshire, U.K.). The porosity was evaluated by two different methods: the density method and the water squeezing method (details in Supporting Information, Table S1). The presence of GO coating onto aerogels was observed with SEM (ZEISS LEO 1530 FEG, Germany), operated at 5 kV and secondary electrons were collected by means of an In-Lens detector.

2.3 X-Ray Photoelectron spectroscopy (XPS)

The aerogels were cut in 1 mm thin slice and fixed on conductive carbon tape for X-Ray Photoelectron analysis. The XPS spectra were recorded with a Phoibos 100 hemispherical energy analyser (Specs, Germany) using Mg Kα radiation (ħω = 1253.6 eV; X-Ray power = 125W) in constant analyser energy (CAE) mode, with analyser pass energies of 10 eV and overall resolution of 0.9 eV on Ag 3d peak. The base pressure in the analysis chamber during analysis was $2 \cdot 10^{-9}$ mbar. All spectra were calibrated to the C 1s binging energy (285.0 eV). Spectra were fitted by using CasaXPS data analysis software (www.casaxps.com). The atomic % were obtained from survey spectrum, while the shape of C 1s peak was acquired in order to identify the C-O and C-N present.

2.4 Adsorption of ofloxacin and ciprofloxacin

Kinetic experiments were performed in batch by dispersing the selected material (50 mg) in 10 mL of solution of ofloxacin and ciprofloxacin mixture (0.5 mg/L each) and mixing with rotator stirred speed 32 rpm in darkness and the solutions analyzed at selected intervals (1, 4 and 24 h).

For isotherm experiments of ofloxacin a stock solution at 500 mg/L in tap water was prepared. Adsorption experiments were performed by dispersing 50 mg of the selected material in 10 ml of ofloxacin solution (tap water) at 0.5, 5, 25, 50, 250, 500 mg/L, prepared by dilution of the stock solution and mixed (32 rpm) for 24 h.

For isotherm experiments of ciprofloxacin, a stock solution at 250 mg/L in tap water was prepared. Adsorption experiments were performed by dispersing 50 mg of the selected material in 10 ml of ciprofloxacin solution (tap water) at 0.5, 5, 25, 50, 250 mg/L, prepared by dilution of the stock solution and mixed (32 rpm) for 24 h.

Antibiotics were detected by HPLC (Dyonex Ultimate 3000) system equipped with a diode array detector. Automated injection volume was 0.2 mL. LC-MS grade acetonitrile was purchased from Sigma-Aldrich at the highest available purity and used without any further purification. Ultrapure water (18.2 MΩ/cm at 25 °C, Millipore Milli-Q system) was used. The chromatographic separation was performed on a reverse phase Zorbax C8 column 4.6 x 150 mm, 5 μm, at flow rate of 1.0 mL/min and detection performed , at maximum UV absorption of the selected analyte (details in Table S1-2 in SI). In all experiments the removal of analytes was determined by comparison with untreated solution.

2.5 Adsorption of lead

Kinetic adsorption of Pb was studied in batch tests by dispersing the selected material (about 40 mg) in 40 ml of 100 μg/L Pb solution (Milli-Q water, pH 7). Solutions were mildly shaken onto orbital shaker (160 osc/min) and samples (2 ml taken by syringe without filtering) were taken at selected interval (1, 3 and 24 h).

Adsorption isotherms in batches were carried out to evaluate efficiency of different materials to remove Pb. One sample, previously equilibrated in Milli-Q, was weighed (range 40-50 mg) and added to Milli-Q solutions (40 ml in Falcon) spiked at different levels of Pb (0-20 mg/L) using Pb stock solution (1 g/L, Fluka). pH was initially adjusted to pH 6.5 ±0.5. Solutions were mildly shaken onto orbital shaker (160 osc/min) for 24 h. 2 ml of samples were taken by syringe without filtering.

All samples for adsorption studies (kinetic and isotherm) were run in duplicate, mean and standard deviation reported. Pb was measured by Atomic Absorption Spectrometer (AAS, AAnalyst800, Perkin Elmer) onto Ir-coated furnace.

After last isotherm level, a release test of adsorbed Pb was performed to evaluate if strong chemio-sorption was the mechanism involving Pb removal or it was more pore diffusion into nano-porous sponge structure. Each aerogel was put into 10 ml Milli-Q (3 times, R1, R2 and R3 namely) and shaken at 240 osc/min. Pb released was analyzed after 30 min contact time (R1 and then R2) and after 48 hours (R3). A cumulative % release value is given comparing mass release to adsorbed amount.

2.6 Adsorption models

Adsorption process was described by three different models Freudlich, Langmuir and BET, usually the most suitable to mimic pollutants equilibria with the adsorbent phase (Foo and Hameed, 2010; Limousin et al., 2007). Freundlich empirical model considers adsorption sites at different energies with stronger binding sites firstly occupied, while Langmuir model is based on experimental evidences and it describes solute-adsorbent equilibrium by assuming a monolayer coverage with all sites energetically equally probable. BET model is based on the assumption that exists a multilayer coverage and represents an extension of Langmuir model. A detailed model and relative parameters description are provided by Casentini et al., (2019). Briefly, we summarize hereafter used equations:

Freundlich Model $$q_e = K_f C_e^{1/n} \quad (1)$$

where q_e is the measured equilibrium adsorption capacity ($mg/g_{adsorbent}$), C_e is the measured equilibrium solute concentration (mg/L), K_f is an indicator of the adsorption capacity (L/mg) and 1/n is an indicator of adsorption intensity.

Langmuir Model $$q_e = \frac{q_{max} b C_e}{1 + b C_e} \quad (2)$$

where q_e is the measured equilibrium adsorption capacity ($mg/g_{adsorbent}$), C_e the equilibrium solute concentration (mg/L), q_{max} corresponds to the maximum adsorption capacity of a monolayer stratum ($mg_{Pb}/g_{adsorbent}$) and b is Langmuir coefficient (L/mg).

BET model
$$q_e = \frac{K_b C_e q_{max}}{(C_s - C_e)[1+(K_b-1)\frac{C_e}{C_s}]} \quad (3)$$

where q_e is the measured equilibrium adsorption capacity ($mg/g_{adsorbent}$), C_e is the measured equilibrium solute concentration (mg/L), C_S is solute concentration saturating first layer (mg/L), q_{max} is the maximum adsorption capacity of a monolayer stratum ($mg/g_{adsorbent}$) corresponding to Langmuir model.

The goodness of fit was then evaluated by calculating the coefficient of determination (R^2) and the Root Mean Square Error (RMSE), as described in Casentini et al. (2019).

2.7 Flow cytometry

Samples were collected in 2-mL Eppendorf safe-lock tubes and analyzed soon after sampling. Groundwater used for the test was collected from a nearby well. The natural groundwater non-pathogenic microbial community characterization was estimated by the Flow Cytometer A50-micro (Apogee Flow System, Hertfordshire, England) equipped with a solid-state laser set at 20 mV and tuned to an excitation wavelength of 488 nm." Following previously published protocols (Amalfitano et al., 2018), the volumetric absolute cell counting was carried out by staining with either SYBR Green I (1:10000 final dilution; Molecular Probes, Eugene, OR, USA) or SYBR Green I and Propidium Iodide (PI= 10 μg/mL final concentration) for 10 min in the dark at room temperature. The light scattering signals (forward and side scatters), the green fluorescence (530/30 nm) and red fluorescence (>610 nm) were acquired for the single cell characterization. Thresholding was carried out using the green channel. Samples were run at low flow rates to keep the number of events below 1000 event s^{-1}. The data were analyzed using the Apogee Histogram Software (v89.0). The total cell counts were determined by signatures in a plot of the side scatter vs

305 the green fluorescence. Live and dead cells were differentiated in a plot of green vs red
306 fluorescence. Viable cells showed higher green fluorescence signals than the membrane
307 compromised dead cells selectively marked in red by PI (Amalfitano et al., 2009).
308
309 **3. Results and Discussion**
310 **3.1 Synthesis and morphologies of CGGO aerogels**
311 Chitosan-Gelatin-GO aerogels (CGGO) and their control samples (CG) were prepared by a
312 blending-freeze drying based approach. Moreover, to obtain stable aerogels in wet condition a
313 physical cross-linking, dehydrothermal treatment (DHT), was carried out. Indeed, as previously
314 demonstrated, due to the temperature and vacuum condition of DHT process, covalent amidic bonds
315 between gelatin and chitosan are created upon DHT process, this increasing the chemical and
316 mechanical robustness of the final aerogel (Campodoni et al., 2019).
317 For the preparation of the GO embedded aerogel, CGGO-E, GO was introduced in the polymeric
318 hydrogel before gelation and freeze-drying. The dried composite CGGO-E, aerogel underwent DHT
319 treatment for further stabilization at 100 °C to prevent reduction of GO (Backes et al., 2020). The
320 control sample CG-E was prepared under the same experimental conditions.
321 On the other hand, for the preparation of GO coated aerogel CGGO-C, a GO suspension was
322 dropped on an already DHT stabilized aerogel. For both embedded and coated aerogels the ratio
323 GC:GO in the blend was about 2% w/w of GO. Details on the preparation conditions are reported in
324 the experimental section and in Fig. S1.
325 The macroscopic images of the aerogels and their morphologies at different magnification are
326 shown in Fig. 1 and Fig. S2. GO free aerogels showed a pale yellow colour while as expected, a
327 dark colour was observed after the addition of GO in both embedded and coated samples.
328 On the other hand, large tubular pores featured by aligned channels were observed for all samples
329 independently on the presence of GO, this being beneficial for water permeation. Density
330 experiments (see Table S1) were also carried out to estimate the porosity. Control samples CG-E

and CG-C showed a porosity higher than samples with GO. Furthermore, GO coated samples revealed a porosity lower than the GO embedded ones (Fig. 1).

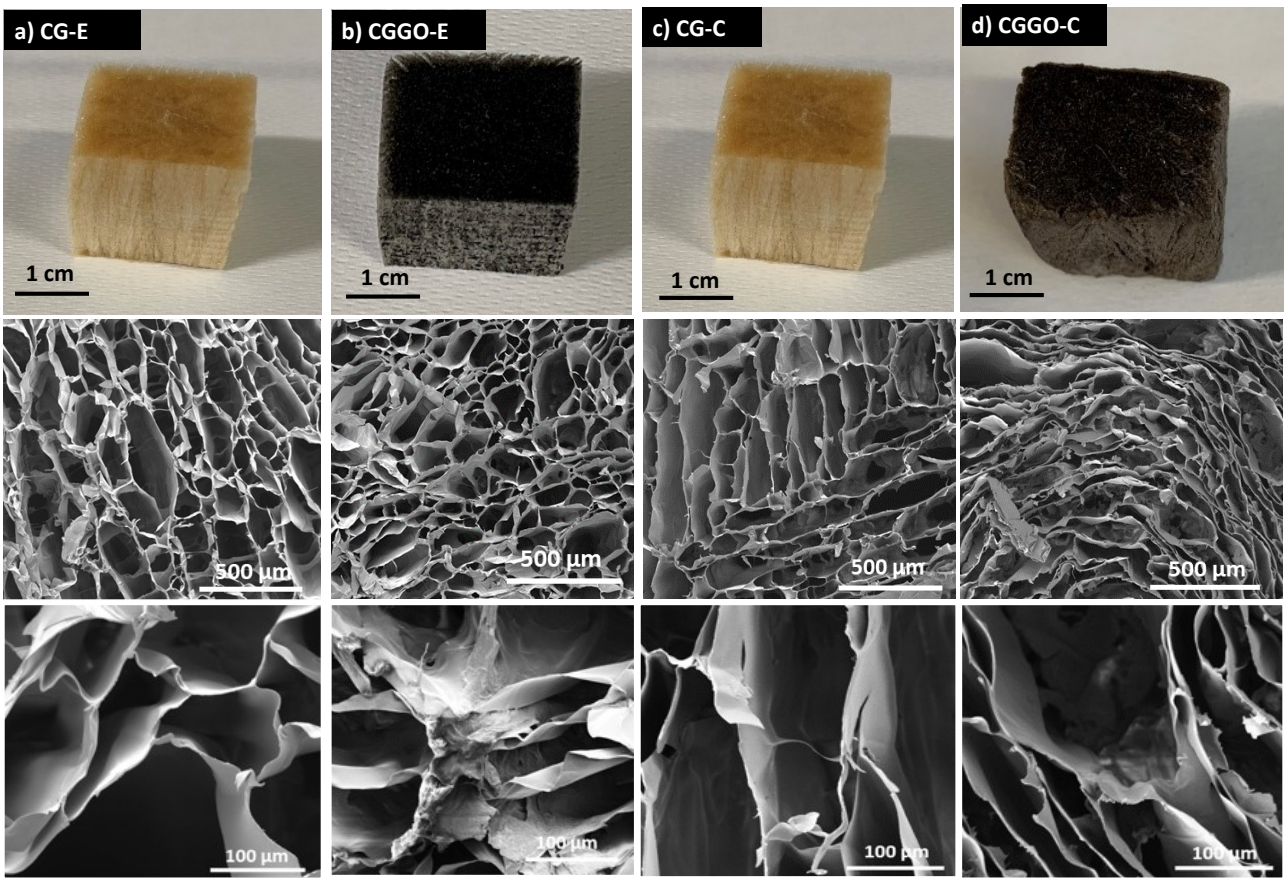

Fig. 1. ESEM images of cross-sections at different magnifications of polymeric (CG-E, CG-C) and composite (CGGO-E, CGGO-C) aerogels. Aerogels up to 20 cm sized were prepared.

A GO continuous film with thickness in the order of magnitude of tens of nm was expected in CGGO-C aerogel (Fig. 2), similar to our previous coating of polysulfone hollow fibers (Kovtun et al., 2019a). Wrinkle typically related to GO were clearly visible and not observed in CG-G control samples, which showed a smooth surface. The GO coating was even more visible at high magnification in proximity of few micrometre large crevice (Fig. 2 c,d), where the coating was partially detached from surface.

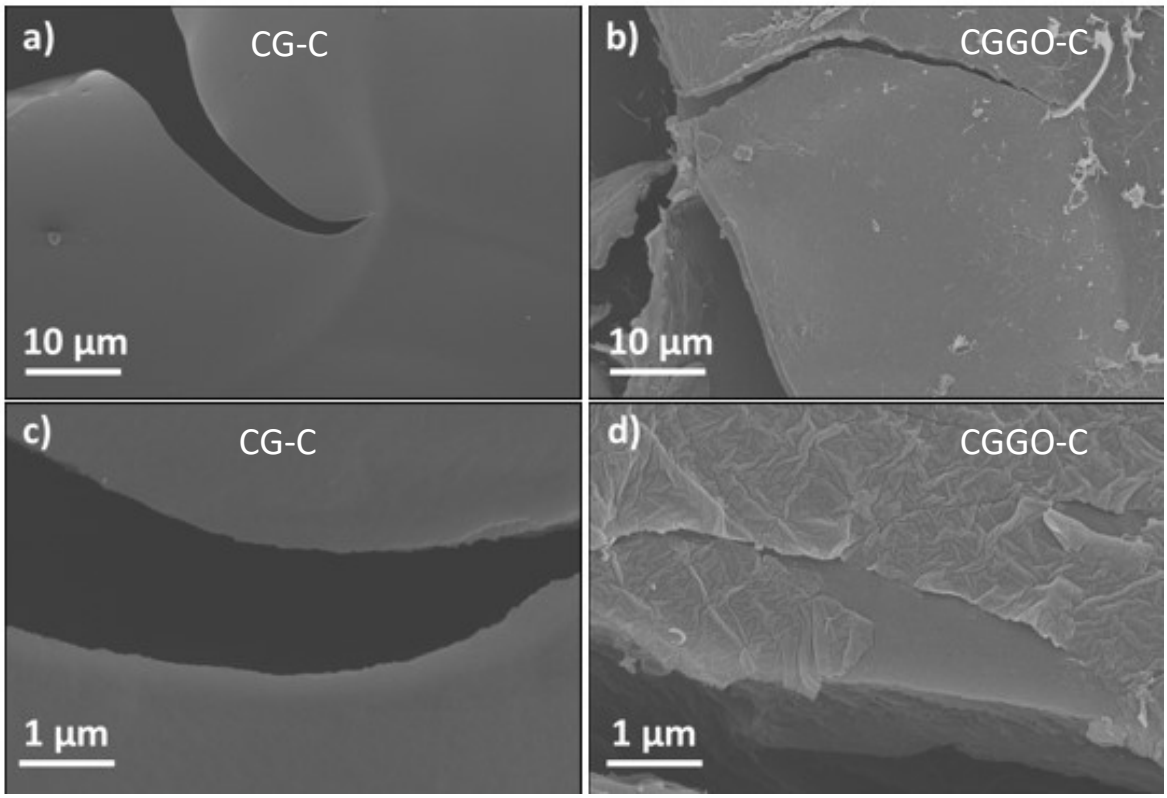

Fig. 2. FEG-SEM images of CG-C (a,c) and CGGO-C (b,d).

The stability of GO doped aerogels was tested by monitoring the GO release in water after 24 h of static contact. GO release was evaluated by UV-Vis spectroscopy in comparison to GO standard solutions. No evidence of GO was found in case of CGGO-E/C, hence we excluded any release at least in the detection limit range of UV-Vis spectroscopy (about 2 mg/L) (Kovtun et al., 2020; Kovtun et al., 2019a) for both embedded and coated aerogels (Fig. S3).

3.2 X-ray photoelectron spectroscopy (XPS)

XPS experiments were performed to check if the fabrication process induced GO changes, i.e. reduction to graphene. Survey spectra showed the signal form C 1s, N 1s and O 1s transitions (Fig. 3). The measured atomic % were close to those reported by Maachou et al. (2013) for pristine chitosan (C:O: N = 63.6: 29.2: 7.3). The binding energy (B.E.) of O 1s and N 1s peaks were in excellent agreement with literature, respectively 532.7±0.1 and 399.5±0.1 eV and the high-resolution C 1s peak confirmed the chemical structure of chitosan (Maachou et al., 2013): one C-C

group (284.8 eV), one O-C-O group (287.7 eV), while the three C-O and the C-N carbons present the same B.E. (286.2 eV). The measured C 1s signal (Fig. S4) was in good agreement with literature, C-C peak is at 284.8±0.1 eV, C-O/C-N at 286.4±0.1 eV and O-C-O at 287.9±0.1 eV, the relative abundances of carbon functional groups were close to pure chitosan. However, the amount of C-C carbon is slightly higher respect to the theoretical value, probably due to residual from gel and/or to the atmospheric contaminations (samples were stored in air).

The C 1s signal from CG-B, CGGO-B and CG-C featured the same shape and could be associated to the chemical structure of chitosan, while the C 1s of CGGO-C showed a completely different shape, not compatible with chitosan: the presence of aromatic and aliphatic C-C bonds at c.a. 285 eV and the peak at 286.7 eV indicated that GO was present in large amount on surface. Consequently, the C 1s peak was fitted by using the model proposed for GO (Kovtun et al., 2019b) i.e. aromatic carbon (C=C sp^2, 284.4 eV), aliphatic carbon (C-C sp^3, 285.0 eV), hydroxyl (C-OH, 285.7 eV), epoxy (C-O-C, 286.7 eV), carbonyl (C=O, 288.0 eV), carboxyl (O-C=O, 289.1 eV) and aromatic carbons near vacancies (C-C* sp^2, 283.5) (Larciprete et al., 2012). Moreover, the amount of N 1s was extremely low respect to the other aerogels (1.7 % compared with 10%), this confirming the high coverage of GO on CGGO-C surface.

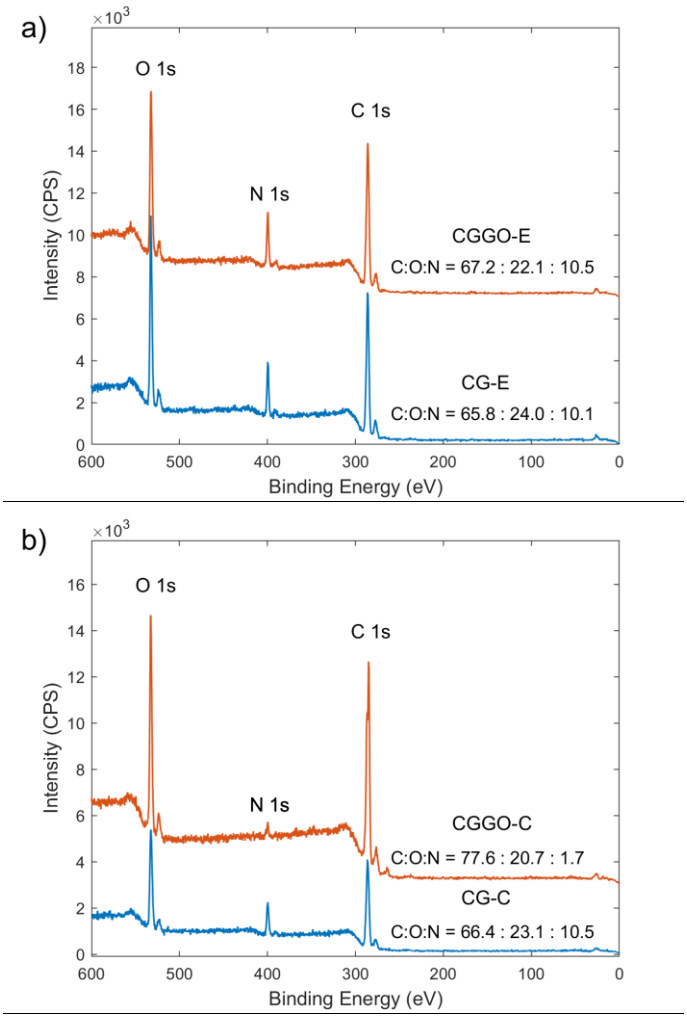

Fig. 3. Survey XPS spectra of a) CG-E and CGGO-E; b) CG-C and CGGO-C. The composition obtained from each spectrum are reported as atomic %.

3.3 Adsorption tests embedded vs coated aerogels

The adsorption kinetic of ofloxacin and ciprofloxacin (Fig. S5) of GO-doped materials and of GO-free control samples was tested over time (1-4-24 h) by dipping an aerogel sample in a solution of the two compounds at 0.5 mg/L in tap water. Negligible adsorption was found for chitosan-gelatin controls even after 24h treatment (figure 4 and fig. S5 for ciprofloxacin). On the other hand, GO embedded aerogels GCGO-E showed removals of 45% and 70% for ofloxacin and ciprofloxacin

respectively after 4 h (see fig. S5 for ciprofloxacin), while GO coated sponges GCGO-C showed a removal around 70% for both compounds already after 1 h treatment.

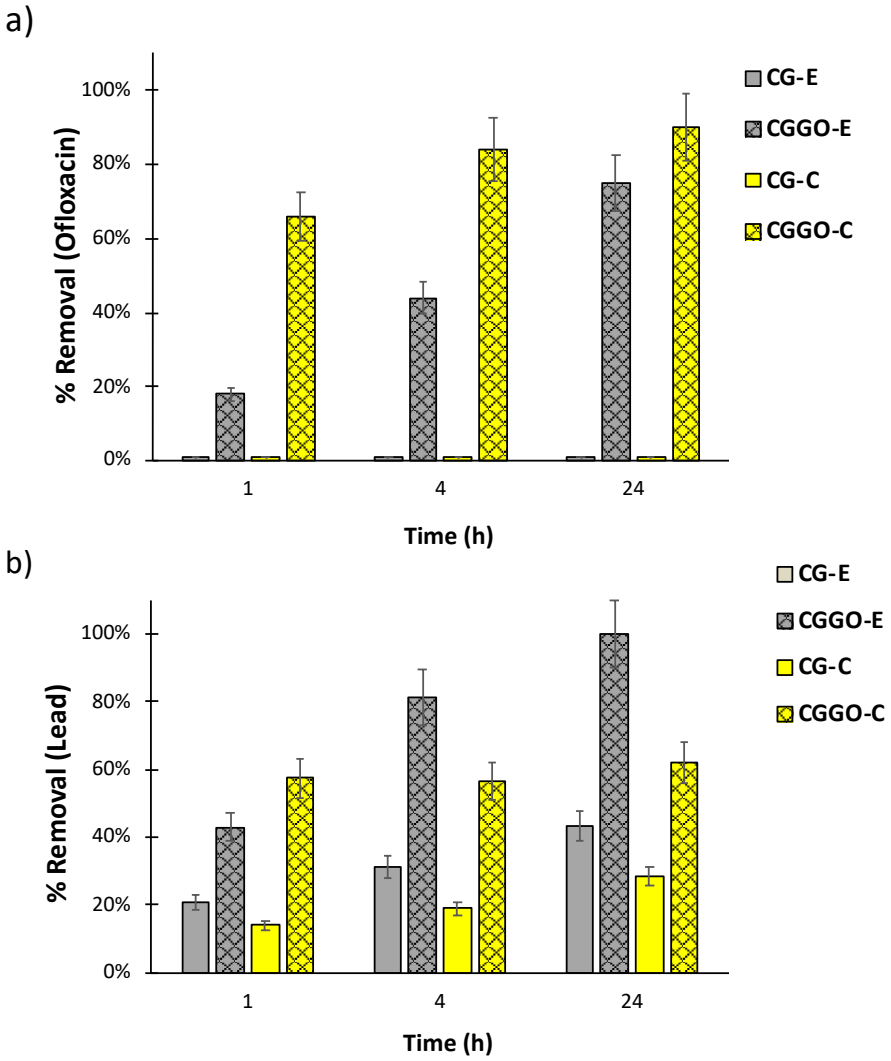

Fig. 4. Kinetics of removal of ofloxacin (a) and Pb (b) by the different samples. The initial concentration of Pb and ofloxacin was 100 µg/L and 500 µg/L, respectively. Kinetic for ciprofloxacin adsorption is shown in Fig. S5.

For both systems the removal of ofloxacin and ciprofloxacin increased with time indeed values up to 80-90% were found after 24 h (see also Fig. S5 for ciprofloxacin), this suggesting that the diffusion of both organic molecules into the aerogel was similar and not very fast.

399 Pb removal efficiency was about 60% and quite stable over time for CGGO-C, while it ranged from
400 43% (1h) to 100% (24 h) for CGGO-E.
401 We conclude that for Pb^{+2} adsorption contact time was not a limiting factor for coated material
402 (CGGO-C), where all adsorption sites are easy reachable on the surface while diffusion into
403 materials becoming very important in embedded material (CGGO-E) where increasing the contact
404 time adsorption increases, indicating that in this case active sites are less promptly available. In
405 control samples (aerogel without GO) negatively charged surface of chitosan also provide good
406 electrostatic attraction for positive Pb (Mishra et al., 2013; Wan et al., 2010) and the removal at an
407 initial concentration of 100 µg/L was 20.8-43.1% in CG-E and 13.9-20.5% in CG-C. Wan et al.
408 (2010) showed that at pH above 4 metals removal by chitosan increased and reached a plateau
409 indicating that at circumneutral pH, as in our case (pH 7) the amino group was deprotonated. At this
410 condition the chelation mechanism outranked the adsorption mechanism where more metal ions
411 chelate with chitosan.
412 Adsorption isotherms experiments were performed to establish the maximum adsorption capacity
413 (see Section 2.4 and 2.5 and results in Table S2 and S3). Different isotherm models were taken into
414 accounts, however as shown by Fig. 5 the adsorption is well described by BET model, indicating a
415 multilayer adsorption, and the difference in performance between bulk (CGGO-E) ad coating
416 (CGGO-C) were negligible with 1^{st} layer maximum adsorption capacity in the range between 4 and
417 8 mg/g in samples with GO (CGGO-E and CGGO-C). In the case of embedded material the 1^{st}
418 layer maximum adsorption q_{max} =4.6 mg/g (ofloxacin) is in agreement with the maximum capacity
419 of polysulfone-GO membranes doped with 5% w/w of GO and obtained by phase inversion
420 (Zambianchi et al., 2017) (i.e. q_{max} 4 mg/g) and it is similar to the maximum capacity of coated
421 sample CGGO-C (8.3 mg/g).

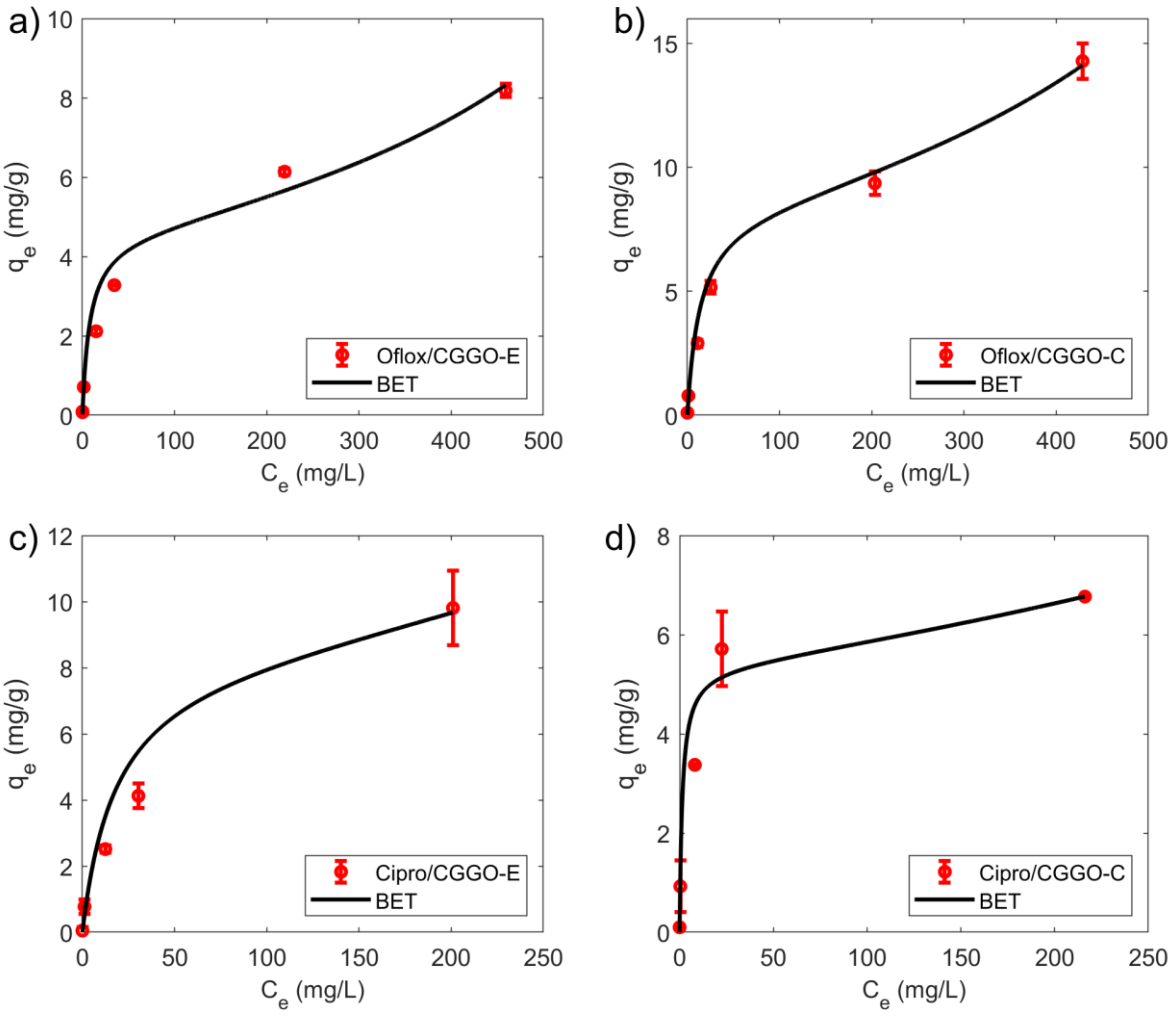

Fig. 5. Adsorption isoterms of Ofloxacin (a,b) and Ciprofloxacin (c,d) of CGGO-E (a,c) and CGGO-C (b,d) samples.

Similarly to organic adsorptions tests, negligible removal was found for GO free samples at these higher concentration. Neverthless, in the case of Pb removal, higher performances were estimated for embedded sample CGGO-E respect to coated one CGGO-C.

Indeed, sample CGGO-E showed highest adsorption efficiency with a BET type behavior reaching a max adsorption monolayer capacity of 11.1 mg/g while in its control without GO q_{max} was only 0.7 mg/g according to Langmuir best fit (Fig. 6). Also, in the sample CGGO-C higher adsorption was observed compared to its control, with monolayer max adsorption capacity 1.5 mg/g and 0.5 mg/g for CGGO-C and CG-C, respectively (see Table S2 for model parameters and selection).

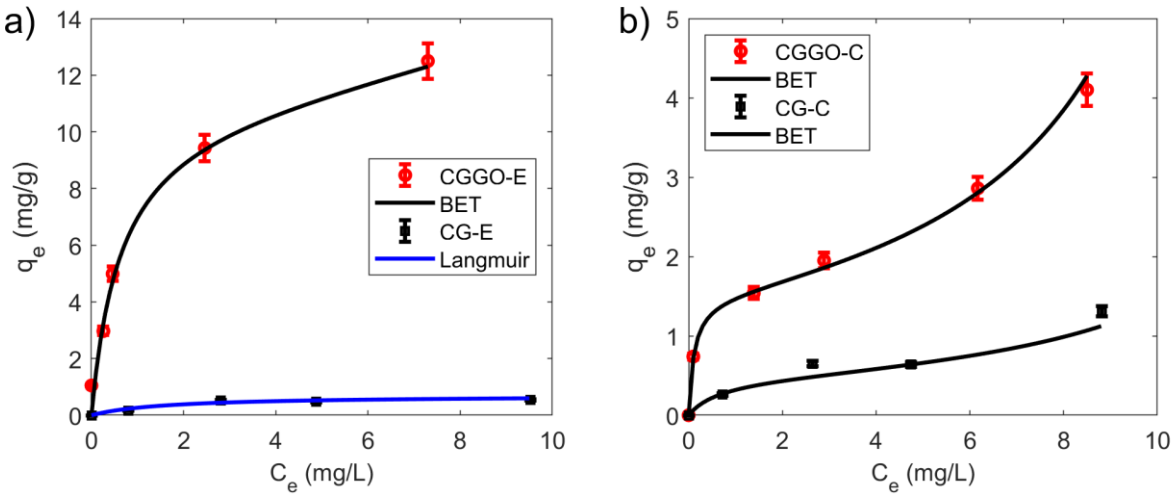

Fig. 6. Pb adsorption onto a) GO embedded aerogel and its control and b) GO coated aerogels and its control. Data are reported as mean values and relative standard deviation. Best fitting prediction model line are reported: BET model and Langmuir Model.

Table 1. Monolayer maximum adsorption capacity (q_{max} in mg/g) of ofloxacin, ciprofloxacin and Pb on all samples. Values from BET adsorption model, except *Langmuir adsorption.

	CG-E	**CGGO-E**	**CG-C**	**CGGO-C**
Ciprofloxacin	<0.1	8.4±0.8	<0.1	5.3±0.5
Ofloxacin	<0.1	4.6±0.5	<0.1	8.3±0.8
Pb	0.7±0.1*	11.1±0.3	0.5±0.1	1.5±0.1

No release of organics was found, while release of the adsorbed Pb was about 7.2 % by CGGO-E and 34.8% by CGGO-C sponge. Therefore, adsorbed Pb is not only higher in embedded aerogels but also more stable. The better performance of embedded aerogels can be likely ascribed to the instauration of stronger monolayer adsorption bonds due to major availability of graphene nanosheets at prolonged contact time while weaker multilayer adsorption at higher initial

concentrations (up to 20 mg/L) for coated aerogels is due to electrostatic repulsions on GO coating surface, as confirmed by BET best fit.

Collectively, embedded systems showed slightly better removal capacity than coated one with respect to the adsorption of both organics and Pb, but adsorption was slower for Pb. No adsorption was observed for control systems CG-E/C in the case of ofloxacin and ciprofloxacin, hence their removal can be totally ascribed to GO. On the contrary, Pb adsorption was also observed not coated aerogels due electrostatic attraction and amino group chelation of chitosan, nevertheless GO coating raised significantly their removal efficiency.

3.4 Microbial removal efficiency and viability assessment

Flow cytometry was used as a rapid tool to assess the removal of the total microbial cells by filtering waters through the aerogels (i.e. inlet vs outlet waters). Moreover, the microbial viability was evaluated considering the increase of membrane-damaged cells in comparison to the control treatment. The performances of the new materials were evaluated by flow cytometry considering the changes in total cell counts (TCC) and membrane integrity (% of dead cells over the total) between the source and the filtered waters. The microbial water quality assessment of nonpathogenic microorganisms through flow cytometry can be applied to determine the effectiveness of water filtration treatments, also facilitating the optimization of reclamation procedures in experimental and pilot studies and the upscaling to full-scale plants (Safford et al., 2019; Vergine et al., 2020).

In this study, TCC increased only slightly over time in comparison to the control sample with no treatment, but without significant differences between treatments at 24h of incubation. The CG aerogels were likely to provide substrates suitable for microbial growth. However, potential antimicrobial effects were clearly visible already at 1h in CGGO-C, with an increase of one order of magnitude of membrane-compromised cells in comparison to the control. Interestingly at 24 h, a net increase of dead cells was observed in all treatments (Fig. 7). The major antimicrobial effect

observed at CGGO-C suggested that homogeneous GO coating on the sponge surface was more effective in damaging cell membranes at the microbial community level than the GO-embedded within the sponges. Our findings are in line with previous observations reported by testing pure microbial cultures (Liu et al., 2018).

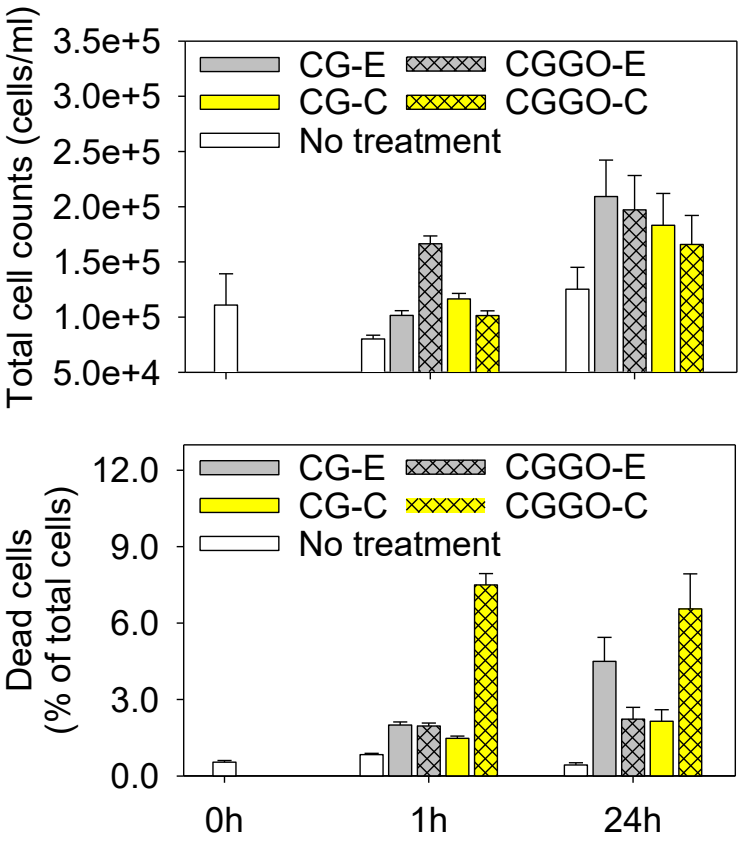

Fig. 7. Flow cytometric characterization of the water microbial community upon filtration through CG and CGGO aerogels. The total cell counts, and the percentage of dead cells were assessed after 1h and 24h from filtration. "No treatment" refers to water sample with no sponge.

5. Conclusions

In summary, we reported the fabrication of novel eco-sustainable aerogels made by chitosan-gelatin, CG, and GO and their characterization as adsorbent for water purification. We compared two different composites polymer-GO (2% w/w) consisting of i) bulk aerogels with GO embedded

490 in the porous matrix and ii) aerogel coated with a GO layer. Adsorption tests performed on selected
491 fluoroquinolonic antibiotics and Pb contaminants showed faster adsorption for GO coated samples,
492 especially for Pb ions. Similar maximum adsorption capacity between GO embedded and GO
493 coated materials was observed with respect to fluoroquinolonic antibiotics. On the contrary, in the
494 case of Pb the adsorption efficiency was significantly higher (one order of magnitude) and stronger
495 in embedded samples where monolayer adsorption capacity was described by Langmuir model.
496 Collectively these results show that both GO embedding and coating are valuable strategies to
497 exploit GO sorption capability through hydrophobic (GO-organics) or electrostatic (GO-Pb)
498 interactions. For antibiotics removal, the amount of GO seems the key factor to maximize the
499 removal efficacy while for Pb removal embedding approach seems to work better likely due to
500 instauration of stronger monolayer bonds onto available sites respect to coated samples.
501 In both cases, the comparison with GO free controls demonstrate that adsorption of ofloxacin,
502 ciprofloxacin and Pb can be totally ascribed to GO. Antimicrobial effects were visible already after
503 1h of incubation, with an increase of one order of magnitude of membrane-compromised cells for
504 CGGO-C in comparison to the control, this being of relevance for possible implementation in filters
505 for drinking water.
506 In this work a limited amount of GO (2% w/w) was used for the preparation the targeted
507 coated/embedded structures, but the fabrication procedure developed is compatible with higher GO
508 amounts. This would enhance the removal efficiency up to the maximum capacity allowed by GO,
509 making CGGO aerogels valuable candidates for the realization of truly multifunctional filters for
510 drinking water. Work in this direction is currently under way.
511

512 ## Acknowledgments

513 The research leading to these results has received funding from the European Union's Horizon 2020

research and innovation programme under GrapheneCore2 785219 – Graphene Flagship, POR-FERS 2014-2020 DGR 986/2018 MEDFIL (B54I19000030005) and Italian-PRIN 2017 NANO-CARBOCAT (B54I19002770001) and FLAGERA JTC 2019 (825207)-GO-FOR-WATER.

References and Notes

‡ These authors contributed equally to this work.

Amalfitano, S., Fazi, S., Ejarque, E., Freixa, A., Romaní, A. M., Butturini, A., 2018. Deconvolution model to resolve cytometric microbial community patterns in flowing waters. Cytometry Part A, 93(2), 194-200.

Amalfitano, S., Fazi, S., Puddu, A. 2009. Flow cytometric analysis of benthic prokaryotes attached to sediment particles. Journal of microbiological methods, 79(2), 246-249.

Baig, N., Sajid, I.M., Saleh, T.A., 2019. Graphene-based adsorbents for the removal of toxic organic pollutants: A review. J. Environ. Manage. 244, 370-382.

Barrios, E., Fox, D., Sip, Y. Y. L., Catarata, R. Calderon, J. E., Azim, N., Afrin S., Zhang Z., Zhai, L., 2019. Nanomaterials in Advanced, High-Performance Aerogel Composites: A Review. Polymers, 11, 726.

Backes, C., Abdelkader, A. M. Concepcion, A.et al., 2020. Production and processing of graphene and related materials. 2D Materials, 7, 2, Article Number: 022001.

538 Campodoni, E., Heggset, E. B., Rashad, A., Ramírez-Rodríguez, G. B., Mustafa, K., Syverud, K.,
539 Tampieri, A., Sandri, M., 2019. Polymeric 3D scaffolds for tissue regeneration: Evaluation of
540 biopolymer nanocomposite reinforced with cellulose nanofibrils. Mater. Sci. Eng. C, 94, 867–878.
541
542 Casentini, B., Gallo, M.; Baldi, F., 2019. Arsenate and arsenite removal from contaminated water
543 by iron oxides nanoparticles formed inside a bacterial exopolysaccharide. J. Environ. Chem. Eng. 7,
544 102908.
545
546 Ersan, G., Apul, O.G., Perreault, F., Karanfil, T., 2017. Adsorption of organic contaminants by
547 graphene nanosheets: a review. Water Res. 126, 385-398.
548
549 EU Watch List: https://ec.europa.eu/jrc/en/publication/review-1st-watch-list-under-water-
550 framework-directive-and-recommendations-2nd-watch-list
551
552 Foo, K.Y., Hameed, B.H., 2010. Insights into Modeling of Adsorption Isotherm Systems. Chem.
553 Eng. J. 2010, 156, 2–10.
554
555 Good, K.D., Bergman, L. E., Klara, S.S., Leitch, M. E., Van Briesen, J.M., 2016. Implications of
556 Engineered Nanomaterials in Drinking Water Sources Journal of American Water Works
557 Association- AWWA 108, 1, E1-E17.
558
559 Hartmann, J., Van der Aa, M., Wuijtsa, S., Roda Husmana, A.M., Van der Hoek, J.P., 2018. Risk
560 governance of potential emerging risks to drinking water quality: Analysing current practice.
561 Environ Sci Policy. 84, 97-104.
562

563 Hosseinnejad, M., Jafari, S. M., 2016. Evaluation of different factors affecting antimicrobial
564 properties of chitosan. International journal of biological macromolecules,85, 467-475.
565
566 Ji, K., Han, A., Hirata, A., Fujita, T., Shen, Y., Ning, S., Liu, P., Kashani, H., Tian, Y., Ito, Y.,
567 Fujita, J.I., Oyama, Y., 2019. Lithium intercalation into bilayer graphene. Nat. Commun. 10, 275.
568
569 Joseph, L., Jun, B.M., Flora, J. R.V., Park, C.M., Yoon, Y., 2017. Removal of heavy metals from
570 water sources in the developing world using low-cost materials: A review. Chemosphere. 229, 142-
571 159.
572
573 Kovtun, A., Zambianchi, M., Bettini, C., Liscio, A., Gazzano, M., Corticelli, F., Treossi, E., M. L.
574 Navacchia, Palermo, V., Melucci, M., 2019a. Graphene oxide–polysulfone filters for tap water
575 purification, obtained by fast microwave oven Treatment. Nanoscale, 11, 22780-22787
576
577 Kovtun, A., Bianchi, A., Zambianchi, M., Bettini, C., Corticelli, F., Ruani, G., Bocchi, L., Stante,
578 F., Gazzano, M., Marforio, T. D., Calvaresi, M., Minelli, M., Navacchia, M. L., Palermo, V.
579 Melucci, M., 2020. Core-shell graphene oxide-polymer hollow fibers as water filters with enhanced
580 performance and selectivity, Faraday Discussions, DOI: 10.1039/C9FD00117D.
581
582 Kovtun, A., Jones, D., Dell'Elce, S., Treossi, E., Liscio, A., Palermo, V., 2019b. Accurate chemical
583 analysis of graphene-based materials using X-ray photoelectron spectroscopy. Carbon 143, 268-
584 275.
585 Larciprete, R., Locovig, P., Gardonio, S., Baraldi, A., Lizzit, S., 2012. Dual Path Mechanism in the
586 Thermal Reduction of Graphene Oxide. J. Phys. Chem. C, 116, 9900-9908.
587

588 Krishnakumar, G. S., Gostynska, N., Dapporto, M., Campodoni, E., Montesi, M., Panseri, S.,
589 Tampieri, A., Kon, E., Marcacci, M., Sprio, S., Sandri, M. 2018. Evaluation of different
590 crosslinking agents on hybrid biomimeticcollagen-hydroxyapatite composites for regenerative
591 medicin. Int. J. Biol. Macromol. 106, 739–748.
592
593 Lapworth, D.J., Baran, N., Stuarta, M.E., Warda, R.S., 2012. Emerging organic contaminants in
594 groundwater: A review of sources, fate and occurrence. Environ. Pollut. 163, 287-303.
595
596 Levallois, P., Barn, P., Valcke, M., Gauvin, D., Kosatsky, T., 2018. Public Health Consequences of
597 Lead in Drinking Water. Curr. Environ. Health Rep. *5*, 255–262.
598
599 Limousin, G., J.-P. Gaudet, J.-P., Charlet, L., Szenknect, S., Barthe`s, V., Krimissa, M.,2007.
600 Sorption isotherms: A review on physical bases, modeling and measurement. Appl. Geochem.
601 2007, 22, 249–275.
602
603 Liu, Y., Wen, J., Gao, Y., Li, T., Wang, H., Yan, H., Niu, B., Guo, R., 2018. Antibacterial graphene
604 oxide coatings on polymer substrate. Applied Surface Science 436, 624–630.
605
606 Madadrang, C. J., Kim, H. Y., Gao, G., Wang, N., Zhu, J., Feng, H., Gorring, M., Marc L. Kasner,
607 M. L., Hou, S. 2012, Adsorption Behavior of EDTA-Graphene Oxide for Pb (II) Removal. ACS
608 Appl. Mater. Interfaces, 4, 1186-1193.
609
610 Maachou, H., Genet, M. J., Aliouche, D., Dupont-Gillain C. C., Rouxhet P. G., 2013.
611 XPS analysis of chitosan–hydroxyapatite biomaterials: from elements to compounds. Surf. Interface
612 Anal. 45, 1088–1097.
613

614 Melucci, M., Durso, M., Zambianchi, M., Treossi, E., Xia, Z.-Y., Manet, I., Giambastiani, G.,
615 Ortolani, L., Morandi, V., De Angelis, F., Palermo, V., 2012. Graphene–organic hybrids as
616 processable, tunable platforms for pH-dependent photoemission, obtained by a new modular
617 approach. J. Mater. Chem., 22, 18237-18243.
618
619 Mishra, P. C., Islam M., Patel, R. K., 2013. Removal of Lead (II) by Chitosan from Aqueous
620 Medium. Separation Science and Technology,48:8,1234-1242.
621
622 Mukherjee1, S., Ren, Z., Singh, G., 2018. Beyond Graphene Anode Materials for Emerging Metal
623 Ion Batteries and Supercapacitors. Nano-Micro lett. 10, 70.
624
625 Nappier, S. P., Soller, J. A., & Eftim, S. E., 2018. Potable water reuse: what are the microbiological
626 risks?. Current environmental health reports, *5*(2), 283-292.
627
628 Patrolecco, L., Rauseo, J., Ademollo, N., Grenni, P., Cardoni, M., Levantesi, C., Luprano, M. L.,
629 Barra Caracciolo, A., 2018. Persistence of the antibiotic sulfamethoxazole in river water alone or in
630 the co-presence of ciprofloxacin. Sci. Total Environ. 640–641, 1438–1446.
631
632 Peng, W., Li, H., Liu, Y., Song, S., 2017. A review on heavy metal ions adsorption from water by
633 graphene oxide and its composites. J. Mol. Liq. 230, 496-504.
634
635 Pharmaceuticals in Drinking Water *WHO/HSE/WSH/11.05* [Online] **2011**.
636
637 Poletti, F., Favaretto, L., Kovtun, A., Treossi, E., Corticelli, F., Gazzano, M., Palermo, V., Zanardi,
638 C., Melucci, M., Electrochemical sensing of glucose by chitosan modified graphene oxide, J. Phys.:
639 Mater. 3 (2020) 014011.

Recast of the EU drinking water directive: https://ec.europa.eu/info/law/better-regulation/have-your-say/initiatives/1563-Revision-of-the-Drinking-Water-Directive-RECAST-2017-

Riva, F., Castiglioni, S., Fattorea, E., Manenti, A., Davolia, E., Zuccato, E., 2018. Monitoring emerging contaminants in the drinking water of Milan and assessment of the human risk. Int. J. Hyg. Environ. Health. 221, 3, 451-457.

Roy, S., Edwards, M. A., 2019. Preventing another lead (Pb) in drinking water crisis: Lessons from the Washington D.C. and Flint MI contamination events. Current Opinion in Environmental Science & Health, 7, 34–44.

Safford, H. R., Bischel, H. N., 2019. Flow cytometry applications in water treatment, distribution, and reuse: A review. Water Research,151, 110-133.

Sanseverino, I., Navarro C. A., Loos R., Marinov D., Lettieri T., 2018. State of the art on the contribution of water to antimicrobial resistance. *JRC 114775*.

Shankar, K. G., Gostynska, N., Montesi, M., Panseri, S., Sprio, S., Kon, E., Marcacci, M., Tampieri, A., Sandri, M., 2017. Investigation of Different Cross-Linking Approaches on 3D Gelatin Scaffolds for Tissue Engineering Application: A Comparative Analysis. Int. J. Biol. Macromol. 95, 1199–1209.

Simeonidis, K., Mourdikoudis, S., Kaprara, E., Mitrakas, M., Polavarapu, L., 2016. Inorganic engineered nanoparticles in drinking water treatment: a critical review. Environ. Sci.: Water Res. Technol. 2, 43-70.

Sweetman, M.J., May, S., Mebberson, N., Pendleton, P., Vasilev, K., Plush, S.E., Hayball, J.D., 2017. Activated carbon, carbon nanotubes and graphene: materials and composites for advanced water purification. C. 3, 18.

Tabrizi, N. S., Zamani, S., 2016. Removal of Pb(II) from aqueous solutions by graphene oxide aerogels. Water Sci Technol (1): 74, 256–265.

Troester, M., Brauch. H-J., Hofmann, T., 2016. Vulnerability of drinking water supplies to engineered nanoparticles, Water Research 96, 255-279.

Vergine, P., Amalfitano, S., Salerno, C., Berardi, G., Pollice, A., 2020. Reuse of ultrafiltered effluents for crop irrigation: On-site flow cytometry unveiled microbial removal patterns across a full-scale tertiary treatment. Science of The Total Environment, 718, 137298,

Wan, M.W., Kan, C.C., Rogel, B.D., Dalida, M.L.P., 2010. Adsorption of copper (II) and lead (II) ions from aqueous solution on chitosan-coated sand. Carbohydrate Polymers, 80, 891–899.

Wan, S., He, F., Wu, J., Wan, W., Gu, Y., Gao, B., 2016. Rapid and highly selective removal of lead from water using graphene oxide-hydrated manganese oxide nanocomposites. J. Hazard. Mater. 314, 32-40.

Wang, J., Chen, B., 2015. Adsorption and coadsorption of organic pollutants and a heavy metal by graphene oxide and reduced graphene materials. Chem. Eng. J. 281, 379-388.

691 Westerhoff, P., Atkinson, A., Fortner, J., Wong, M. S., Zimmerman, J., Gardea-Torresdey, Ranville
692 J.J., Herckes, P., 2018. Low risk posed by engineered and incidental nanoparticles in drinking
693 water. Nature Nanotech. 13, 661-666.
694
695 Xu, J., Dou, Y., Wei, Z., Ma, J., Deng, Y., Li, Y., Liu, H., Dou, S., 2017. Recent Progress in
696 Graphite Intercalation Compounds for Rechargeable Metal (Li, Na, K, Al)-Ion Batteries. Adv. Sci.
697 4, 1700146-1700146.
698
699 Xu, J., Cao, Z., Zhang, Y., Yuan, Z., Lou, Z., Xu, X., Wang, X., 2018. A review of functionalized
700 carbon nanotubes and graphene for heavy metal adsorption from water: Preparation, application,
701 and mechanism, Chemosphere 195, 351-364.
702
703 Yang, R., Li, H., Huang, M., Yang, H., Li, A., 2016. A review on chitosan-based flocculants and
704 their applications in water treatment. Water Research, 95, 59-89.
705
706 Yousefi, N., Lu, X., Elimelech, M., Tufenkji, N., 2019. Environmental performance of graphene-
707 based 3D macrostructures. Nature Nanotechn. 14, 107-119.
708
709 Zambianchi, M., Durso, M., Liscio, A., Treossi, E., Bettini, C., Capobianco, M. L., Aluigi, A.,
710 Kovtun, A., Ruani, G., Corticelli, F., Brucale, M., Palermo, V., Navacchia, M. L., Melucci, M.,
711 2017.
712 Graphene oxide doped polysulfone membrane adsorbers for the removal of organic contaminants
713 from water. Chemical Engineering Journal 326, 130-140.
714

715 Zhang, Y. Q., Zhang, M., Jiang, H. Y., Shi, J. L., Li, F. B., Xia, Y. H., Zhang, G. Z., Li, H. J., 2017.
716 Bio-inspired layered chitosan/graphene oxide nanocomposite hydrogels with high strength and pH-
717 driven shape memory effect. Carbohydr. Polym., 177, 116-125.
718
719 Zhou, G., Liu, C., Tang, Y., Luo, S., Zeng, Z., Liu, Y., Xu, R.,Chu, L. 2015. Aerogel-like
720 polysiloxane-graphene oxide gel as a highly efficient and renewable adsorbent for lead and
721 cadmium metals removal from wastewater. Chem. Eng. J. 280, 275-282.
722
723 Zou, X., Zhang, L., Wang, Z., Luo, Y., 2016. Mechanisms of the Antimicrobial Activities of
724 Graphene Materials. J. Am. Chem. Soc. 138, 7, 2064-2077.
725